Computational Simulation and Experimentation of Fluid Flow Characteristics in Expansion U-Loop Model Pipes

Nasaruddin Salam
Mechanical Engineering Department, Faculty of Engineering, Hasanuddin University, Gowa, Indonesia
nassalam.unhas@yahoo.co.id

Rustan Tarakka
Mechanical Engineering Department, Faculty of Engineering, Hasanuddin University, Gowa, Indonesia
rustan_tarakka@yahoo.com

Bambang Bakri
Civil Engineering Department, Faculty of Engineering, Hasanuddin University, Gowa, Indonesia
bambangbakri@gmail.com

Lukman Kasim
Mechanical Engineering Department, Faculty of Engineering, Hasanuddin University, Gowa, Indonesia
lukman.kasim@unhas.ac.id (corresponding author)

Muhammad Hidayat Bin Jamal
Faculty of Engineering, School of Civil Engineering, University Teknologi Malaysia (UTM), Malaysia
mhidayat@utm.my

Received: 24 August 2025 | Revised: 15 September 2025 and 11 October 2025 | Accepted: 13 October 2025

 DOI: https://doi.org/10.48084/etasr.14258

ABSTRACT

A pipe's geometry plays a critical role in determining both flow behavior and structural support performance, making it an essential consideration in industrial piping design. Among the various modifications applied in practice, the expansion U-loop is one of the most significant, as it directly influences the pressure losses, flow distribution, and stress conditions. This study investigates the flow characteristics of U-loop expansion pipes through a dual approach that combines computational simulations and experimental testing. The computational study was carried out using Computational Fluid Dynamics (CFD) simulations with ANSYS FLUENT 6.3.26, involving three U-loop models fabricated from galvanized iron, with a wall thickness of 1.2 mm. Two of the models featured equal leg heights, whereas the third employed an asymmetric configuration, with one leg twice the length of the other. To ensure reliability, experiments were conducted under identical boundary conditions at five inlet velocities ranging from 5.0 to 7.0 m/s, with each case repeated three times. Pressure taps were strategically installed along the loop to measure fluid pressure and obtain a detailed distribution profile, particularly at nodes 1, 3, and 7. The results of the simulations and experiments were compared, showing an average validation error of only 3%. The originality of this study lies in combining CFD and direct experimental testing on U-loop models with varied straight-segment lengths, offering valuable insights into the pressure distribution and flow patterns that have not been extensively examined.

Keywords-U-loop pipe expansion; flow pressure distribution; low velocity; pipe hoop stress; longitudinal stress

I. INTRODUCTION

Pipes in fluid systems, especially in the energy, oil, and chemical industries, often include bends, such as U-loop expansions, which significantly affect pressure distribution and pipe stress. Understanding the flow characteristics in U-loop pipes is crucial for preventing damage, leakage, or structural failure and ensuring a safe and efficient design. As an alternative, U-loop expansions help reduce and maintain fluid

pressure, although they also influence the pipe stress, pressure distribution, and flow velocity.

Various experimental and simulation studies have been conducted to estimate the stress and pressure distribution in pipes. For instance, in [1], the stress on U-loop expansion pipes for pertalite fuel distribution was estimated using theCAESAR II software. The stress was mainly caused by the hydrotest, support, and expansion loads. All stress remained below standards, confirming that the pipe was safe using both computational and theoretical methods [1]. Authors in [2] showed that both symmetrical and asymmetrical expansion loop designs improve flexibility and reduce stress. Given that expansion loops also cause a pressure drop that can increase the pump power and operating costs, CFD simulations were employed to compare four loop types, evaluating the effects of flow velocity, fluid density, and viscosity on the pressure drop, as well as their impact on pump power and additional costs [3].

Studies on expansion loop configurations, including variations in length, shape, and added loops, have investigated static pressure and transient effects, such as water hammer. The results showed that while longer loops reduced the pressure, double or modified loops provided better pressure control in limited spaces. An effective design must balance thermal expansion and transient resistance for reliable system performance [4]. Complementary research using Finite Element Analysis (FEA) with displacement loads on anchors has identified loop variations that minimize the stress from thermal expansion, offering a more efficient design solution [5].

A safe piping system is critical to ensure reliable operation and service life within the design cycle [6]. Permissible stress must account for thermal expansion and occasional loads, with stress values not exceeding allowable limits [7]. Thermal expansion can generate high pipe stress, which can be controlled by expansion loops whose dimensions depend on the material properties, diameter, expansion, and allowable stress. Since no standard definition exists for the loop width (W) and height (H), W/H was varied to theoretically evaluate pipe stress and safety factors [8]. Further optimization of the loop dimensions and supports was performed using ASME B31.3 design guidelines and CAESAR II for stress analysis [9]. The specialized AutoPIPE software was utilized to study rigid and flexible configuration pipe systems and validate that the stresses in pipes and pump nozzles are within the allowable loads [10].

Flow behavior is important in pipe design and has been simulated using CFD to study laminar and turbulent flows, velocity profiles, and pressure distributions under varying Reynolds numbers, geometries, and boundary conditions. 3D CFD models of high-viscosity laminar flow provided consistent velocity and pressure drop results [11]. The CFD analysis of turbulent flow through a 90° pipe bend using ANSYS Fluent, validated by experiments, revealed stronger secondary turbulence and a higher RMS velocity near the outer wall, peaking at 45° owing to vortical circulation, along with increased static pressure and turbulent viscosity at the bend [12]. The k–ε turbulence model has also been applied using CFD simulations [13, 14].

Detecting leaks in oil and gas pipeline networks is important for maintaining the efficiency and reliability of fluid distribution. It has been shown that pressure is the most accurate parameter for identifying leakages in pipes [15]. CFD simulations have been employed to study the pressure drop caused by leaks in 90° elbow pipes [16] and demonstrate that leaks with a high rate or a position closer to the inlet result in a smaller pressure drop [17]. Computational analysis shows that the piping system is safe because the operational stress has a ratio of ≤ 1 to the permissible limit according to standards, with two main failure modes, namely continuous stress (primary) and expansion (secondary) [18]. Authors in [19] used CFD through a modified SIMPLE solver on OpenFOAM, emphasizing the leak detection in inclined pipes, where the leak rate was influenced by the position and angle of the pipe, and was higher at the inlet and on large slopes. Additionally, a mathematical model based on dimensionless variables and orientation angles was developed to accurately predict the location of the leaks.

Previous research on U-loop expansion pipes has generally focused on the pressure distribution, stress, and compliance with design standards using computational approaches or ASME B31.3 [7]. However, most studies are still limited to simple configurations and do not explore the effect of variations in the length of straight segments between bends, nor do they provide a comprehensive validation between the numerical results and full-scale experiments. To fill this gap, the present study examines three U-loop pipe configurations with varying straight segment lengths between bends through a combination of CFD simulations and 1:1 scale experimental tests. A comparison of the results provides a more comprehensive picture of the pressure and stress distribution, as well as practical contributions to the design of more reliable industrial piping systems.

II. METHODOLOGY

In this study, experiments and computational simulations were conducted. The experiments were carried out at the Hasanuddin University Fluid Mechanics Laboratory using carbon steel pipe specimens with a diameter of 0.50 inches. CFD simulations were performed using Ansys Fluent 6.3.26 software, modeling steel pipes with an outer diameter of 12.7 mm, a wall thickness of 2.2 mm, and an inner diameter of 8.3 mm with a curved geometry. Three configurations were tested based on variations in the length of the straight segment between the four bends, as shown in Figure 1. In the first configuration (Type 1), the straight segment before each bend was 1 m long with an additional 1 m after the fourth bend. In the second configuration (Type 2), the straight segment consisted of 1 m before the first bend, 0.5 m before the second bend, 1 m before the third bend, 1 m before the fourth bend, and 1 m after the last bend. In the third configuration (Type 3), the straight segment is 1 m before the first turn, 0.5 m before the second turn, 1 m before the third turn, 0.5 m before the fourth turn, and 1 m after the fourth turn. The modeling and meshing processes were performed using Gambit 2.4.6, as displayed in Figure 2. Simulations were performed at five flow velocity levels, namely 5.0 m/s, 5.5 m/s, 6.0 m/s, 6.5 m/s, and

7.0 m/s, to analyze the flow characteristics inside a pipe with an elbow geometry.

All tests were conducted on a 1:1 scale, such that the dimensions of the model represented the actual conditions in the field. The flow velocity variations used for the three types were 5.0, 5.5, 6, 6.5, and 7 m/s.

Figure 1(d) depicts eight pressure measurement points (nodes) placed along the pipe, numbered 1–8. Nodes 1 and 2 were placed before the first bend, nodes 3 and 4 were located on the vertical segment after the first bend, nodes 5 and 6 were located after the second bend, and nodes 7 and 8 were placed at the end of the pipe after the fourth bend. All nodes were connected to a measuring device to obtain data on the pressure distribution of fluid flow. The location markers for each node are explicitly demonstrated to clarify the spatial position of the measuring points, thereby facilitating the process of identifying and analyzing the pressure distribution.

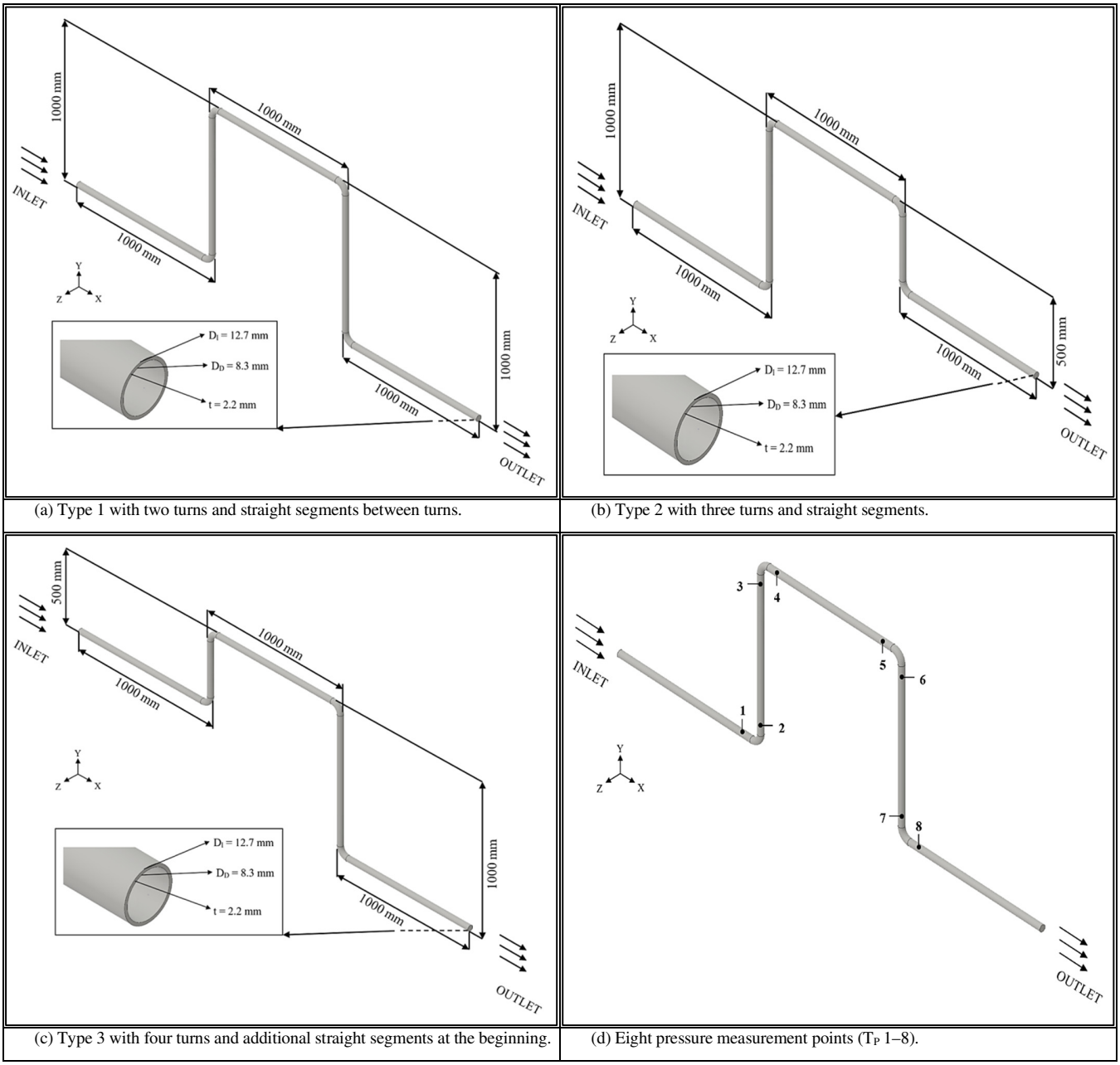

(a) Type 1 with two turns and straight segments between turns.

(b) Type 2 with three turns and straight segments.

(c) Type 3 with four turns and additional straight segments at the beginning.

(d) Eight pressure measurement points (T_P 1–8).

Fig. 1. Dimensions of each U-loop expansion pipe model showing: (a) Type 1 with two turns and straight segments between turns, (b) Type 2 with three turns and straight segments, (c) Type 3 with four turns and additional straight segments at the beginning, and (d) Eight pressure measurement points (TP 1–8).

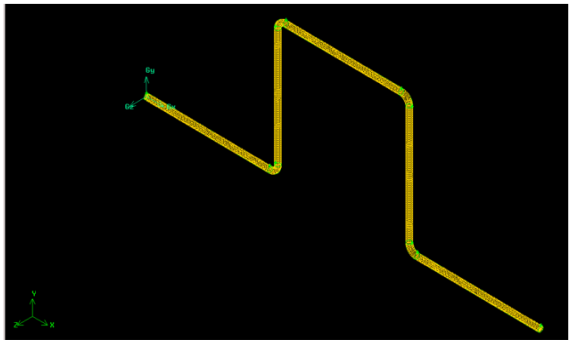

Fig. 2. Computational meshing of the U-loop pipe expansion.

The boundary conditions in the simulation were determined based on the flow modeling requirements in the pipe and were adjusted to the parameters used. Details regarding the boundary conditions applied are presented in Table I.

The hoop stress (σ_h) equation was used to analyze and determine the stress characteristics acting on the pipe wall owing to the internal pressure. It is expressed by [20]:

$$\sigma_h = \frac{p\,D}{2\,t} \quad (1)$$

where p is the internal pressure, D is the pipe diameter, and t is the pipe wall thickness.

Meanwhile, the longitudinal stress (σ_l), which is the axial stress acting along the pipe axis due to internal pressure, is determined by [20]:

$$\sigma_l = \frac{p\,D}{4\,t} \quad (2)$$

TABLE I. BOUNDARY CONDITIONS OF EXPANSION U-LOOP PIPE MODEL

Boundary conditions	Type	Value
Fluid (water) properties	Density	779.1 kg/m^3
	Viscosity	0.0005088 kg/m.s
Inlet	Velocity inlet	5.0, 5.5, 6.0, 6.5, and 7.0 m/s
Outlet	Pressure outlet	
Model	Wall	

III. RESULTS AND DISCUSSION

The computational results for the pressure distribution were obtained by applying the same treatment to five levels of the water flow velocity (V): 5.0, 5.5, 6.0, 6.5, and 7.0 m/s. The computational results for Types 1, 2, and 3 are presented in Tables II, III, and IV, respectively. Based on the computational simulation results in Tables II-IV, the maximum pressure drop between the inlet and outlet sides of the water flow in the U-shaped expansion pipe, ΔP=P1-P8, is 95,621 Pa for Type 1 and V = 7.0 m/s, while the smallest pressure drop is 60,668 Pa for Type 2 and V = 5.0 m/s.

TABLE II. COMPUTATIONAL RESULTS OF PRESSURE DISTRIBUTION IN A TYPE 1 U-LOOP EXPANSION PIPE WITH VARYING FLOW VELOCITIES

	Flow velocity, V (m/s)	Pressure distribution at each elbow, P (Pa)								ΔP (P1-P8)
		Elbow 1		Elbow 2		Elbow 3		Elbow 4		
		1	2	3	4	5	6	7	8	
Type 1	5.0	80619	66578	54454	48413	38289	34248	29124	18083	62536
	5.5	92149	77339	62909	58099	43670	38860	34430	21620	70529
	6.0	103878	88286	71511	65919	49143	43551	36776	25184	78694
	6.5	114977	101445	81850	75318	55722	49191	39595	28064	86913
	7.0	130332	112976	90910	83555	61488	54133	42066	34711	95621

TABLE III. COMPUTATIONAL RESULTS OF PRESSURE DISTRIBUTION IN A TYPE 2 U-LOOP EXPANSION PIPE WITH VARYING FLOW VELOCITIES

	Flow velocity, V (m/s)	Pressure distribution at each elbow, P (Pa)								ΔP (P1-P8)
		Elbow 1		Elbow 2		Elbow 3		Elbow 4		
		1	2	3	4	5	6	7	8	
Type 2	5.0	74001	63335	55778	43001	32001	28334	21000	13334	60668
	5.5	83673	71295	60782	49404	36269	31891	23135	15756	67917
	6.0	94931	81802	66287	56158	40772	35644	25386	20157	74773
	6.5	106006	92139	76670	62803	45202	39335	27601	23734	82272
	7.0	119886	104160	82257	70531	50354	43629	31177	29451	90434

TABLE IV. COMPUTATIONAL RESULTS OF PRESSURE DISTRIBUTION IN A TYPE 3 U-LOOP EXPANSION PIPE WITH VARYING FLOW VELOCITIES

	Flow velocity, V (m/s)	Pressure distribution at each elbow, P (Pa)								ΔP (P1-P8)
		Elbow 1		Elbow 2		Elbow 3		Elbow 4		
		1	2	3	4	5	6	7	8	
Type 3	5.0	76605	71898	58484	50777	39656	35949	18121	15414	61191
	5.5	86493	82127	68394	58028	44930	40563	20099	17732	68761
	6.0	98863	89738	75490	66366	50993	45869	22373	22248	76614
	6.5	109976	95007	81149	75220	57433	51504	22787	25858	84118
	7.0	124663	104885	91330	84553	64220	57443	30333	31555	93108

Figures 3-5 present the relationship between the pressure distribution (P) and each measurement point position at the elbow (T_P), with a similar characteristic pattern in all types of U-Loop expansion pipes being observed. The pressure decreases gradually from T_P 1 to T_P 8. The same pattern is also noted when the velocity varies.

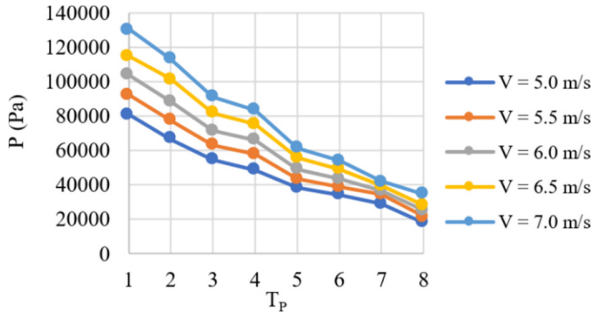

Fig. 3. Computational results of P against T_P of a Type 1 U-loop expansion pipe with varying V.

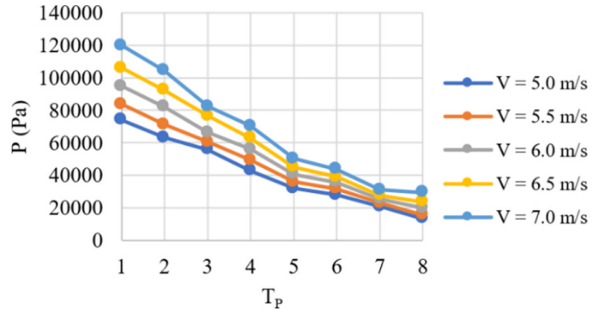

Fig. 4. Computational results of P against T_P for Type 2 U-Loop expansion pipe with varying V.

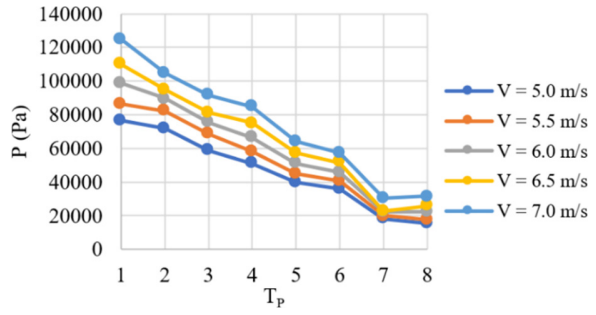

Fig. 5. Computational results of P against T_P for Type 3 U-Loop expansion pipe with varying V.

The ΔP values for the three types at each flow velocity are compared in Table V. From Table V, it is evident that for all flow velocities, Type 2 exhibits the smallest pressure drop, whereas the largest pressure drop occurs in Type 1. This indicates that to mitigate water flow pressure, Type 1 is the most suitable for application, followed by Type 3, and finally Type 2. Figure 6 illustrates the relationship between ΔP and V for each type of U-Loop expansion pipe. In general, the characteristic pattern is similar for all types of U-Loops, where the ΔP increases with increasing flow velocity. The computational results in Table V and Figure 6 also indicate that there are variations in the amount of pressure drop at the same velocity for each type of U-Loop. For example, at a V of 7 m/s, the ΔP is 95,621 Pa for Type 1, 90,434 Pa for Type 2, and 93,108 Pa for Type 3. These findings reveal that the pressure drop is not only influenced by the number of elbows but also by the distance and configuration of the positions between elbows.

TABLE V. COMPUTATIONAL RESULTS OF PRESSURE DROP FOR THE 3 TYPES OF U-LOOP EXPANSION PIPES AND VARYING FLOW VELOCITY

Flow velocity, V (m/s)	Flow pressure drop, ΔP (P1-P8), Pa		
	Type I	Type II	Type III
5.0	62536	60668	61191
5.5	70529	67917	68761
6.0	78694	74773	76614
6.5	86913	82272	84118
7.0	95621	90434	93108

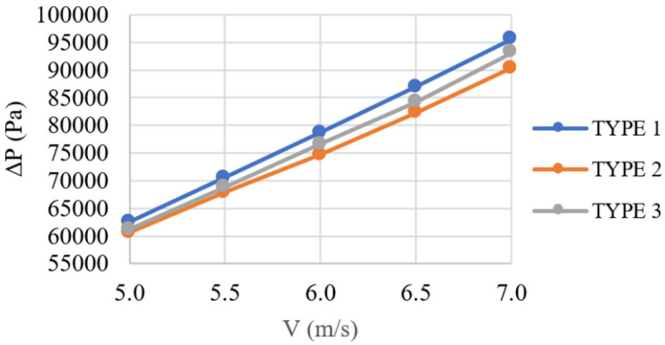

Fig. 6. Computational results of ΔP against five levels of V for each type of U-loop expansion pipe.

The results of the pressure distribution experiments were obtained by applying five water flow velocity levels: 5.0, 5.5, 6.0, 6.5, and 7.0 m/s. The experimental results are presented in Tables VI-VIII for Types 1-3, respectively. The maximum pressure drop between the inlet and outlet sides of the water flow in the U-shaped expansion pipe–loop pipe was 92,000 Pa for Type 1 and V = 7.0 m/s, whereas the smallest pressure drop ΔP was 59,000 Pa for Type 2 and V = 5.0 m/s.

TABLE VI. EXPERIMENTAL RESULTS OF PRESSURE DISTRIBUTION IN A TYPE 1 U-LOOP EXPANSION PIPE WITH VARYING FLOW VELOCITIES

	Flow velocity, V (m/s)	Pressure distribution on each side of the elbow inlet and outlet, P (Pa)								ΔP (P1-P8)
		Elbow 1		Elbow 2		Elbow 3		Elbow 4		
		1	2	3	4	5	6	7	8	
Type 1	5.0	78000	65000	53000	47000	37000	33000	28000	17000	61000
	5.5	89000	76000	61000	57000	42000	37000	33000	20000	69000
	6.0	99000	87000	70000	64000	48000	42000	35000	24000	75.000
	6.5	112000	99000	80000	74000	54000	48000	38000	27000	85000
	7.0	125000	110000	89000	82000	60000	53000	41000	33000	92000

TABLE VII. EXPERIMENTAL RESULTS OF PRESSURE DISTRIBUTION IN A TYPE 2 U-LOOP EXPANSION PIPE WITH VARYING FLOW VELOCITIES

	Flow velocity, V (m/s)	Pressure distribution on each side of the elbow inlet and outlet, P (Pa)								ΔP (P1-P8)
		Elbow 1		Elbow 2		Elbow 3		Elbow 4		
		1	2	3	4	5	6	7	8	
Type 2	5.0	71000	60000	52000	42000	31000	27000	20000	12000	59000
	5.5	80000	70000	59000	48000	35000	30000	22000	14000	66000
	6.0	91000	80000	65000	54000	39000	34000	24000	19000	72000
	6.5	102000	91000	75000	61000	44000	38000	26000	22000	80000
	7.0	115000	102000	81000	69000	49000	42000	30000	28000	87000

TABLE VIII. EXPERIMENTAL RESULTS OF PRESSURE DISTRIBUTION IN A TYPE 3 U-LOOP EXPANSION PIPE WITH VARYING FLOW VELOCITIES

	Flow velocity, V (m/s)	Pressure distribution on each side of the elbow inlet and outlet, P (Pa)								ΔP (P1-P8)
		Elbow 1		Elbow 2		Elbow 3		Elbow 4		
		1	2	3	4	5	6	7	8	
Type 3	5.0	74000	68000	57000	49000	38000	34000	17000	14000	60000
	5.5	83000	81000	67000	57000	43000	39000	19000	16000	67000
	6.0	93000	88000	74000	65000	49000	44000	21000	20000	73000
	6.5	104000	91000	80000	74000	56000	50000	22000	21000	81000
	7.0	118000	102000	90000	83000	63000	56000	30000	29000	89000

Figures 7–9 show the relationship between P and T_P for various flow rates and types of U-Loop expansion pipes. In general, the characteristic patterns obtained are similar for all pipe types, namely the pressure value decreases gradually from T_P 1 to T_P 8, and decreases further as the water flow velocity decreases from 7.0 m/s to 5.0 m/s.

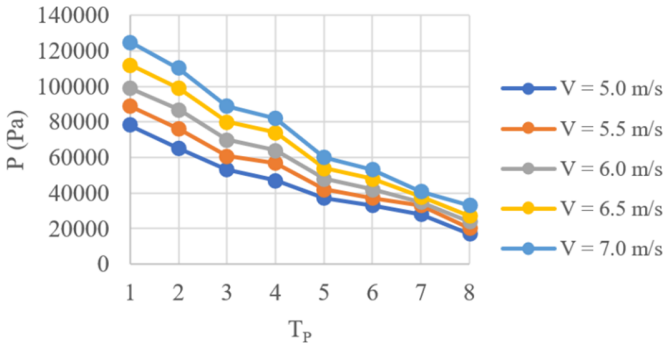

Fig. 7. Experimental results of P against T_P of Type 1 U-Loop expansion pipe with varying V.

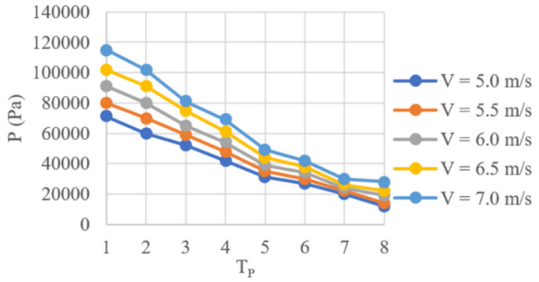

Fig. 8. Experimental results of P against T_P of Type 2 U-Loop expansion pipe with varying V.

Table IX presents the ΔP of the water flow through each U-loop expansion pipe for each flow rate. Type 2 exhibits the lowest pressure drop, whereas Type 1 displays the highest pressure drop. Thus, Type 1 is the most effective in reducing the water flow pressure, followed by Types 3 and 2.

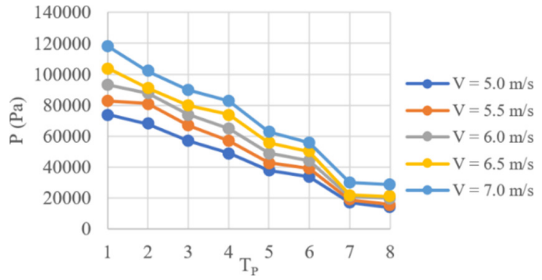

Fig. 9. Experimental results of P against T_P of Type 3 U-Loop expansion pipe with varying V.

TABLE IX. EXPERIMENTAL RESULTS OF PRESSURE DROP FOR THE 3 TYPES OF U-LOOP EXPANSION PIPES AND VARYING FLOW VELOCITY

Flow velocity, V (m/s)	Flow pressure drop, ΔP (P1-P8), Pa		
	Type I	Type II	Type III
5.0	61000	59000	60000
5.5	69000	66000	67000
6.0	75.000	72000	73000
6.5	85000	80000	81000
7.0	92000	87000	89000

Figure 10 shows the relationship between ΔP and V for each type of U-Loop expansion pipe. In general, the characteristic pattern is consistent across all U-Loop types, where the ΔP value increases as the flow velocity increases from 5.0 m/s to 7.0 m/s. The experimental results shown in Table IX and Figure 10 also reveal differences in pressure drop at the same velocity for different U-Loop pipe types. For example, at a V of 7 m/s, ΔP is 92,000 Pa for Type 1, 87,000 Pa for Type 2, and 89,000 Pa for Type 3. These findings confirm that the pressure drop is influenced not only by the number of elbows, but also by the distance and configuration of the position between elbows.

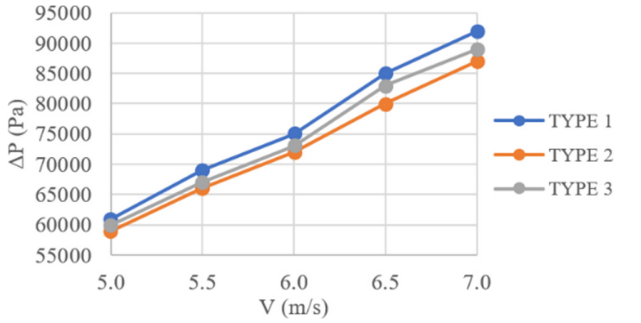

Fig. 10. Experimental change of ΔP with V for all types of U-Loop expansion pipes.

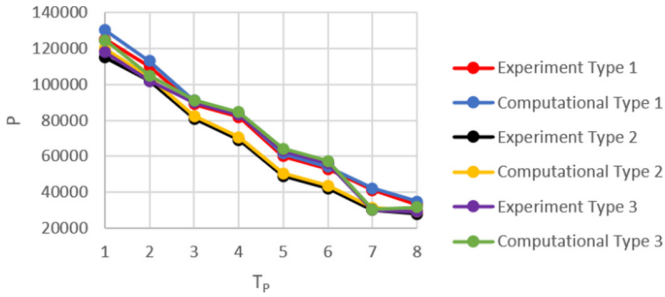

Fig. 11. Distribution of experimental and computational P relative to T_P at V = 7 m/s for all types of U-Loop expansion pipes.

Figure 11 portrays the pressure distributions obtained from the experimental and computational results at a flow velocity of 7 m/s for each U-loop expansion pipe type. Both exhibited similar trends, with an average difference of approximately 4%, and the computational values were consistently higher than the experimental ones at all the measurement points.

Figure 12 shows the ΔP obtained from the experimental and computational results versus V for each U-loop expansion pipe type. Both methods displayed similar trends, with average differences of approximately 3%, while the computational values were consistently higher than the experimental ones.

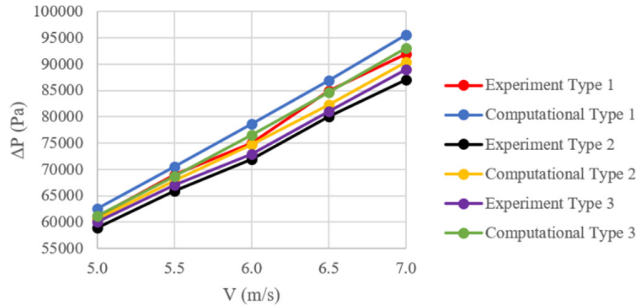

Fig. 12. Distribution of experimental and computational ΔP against V for each type of U-Loop expansion pipe.

Figures 13 and 14 show the relationship between the hoop stress drop ($\Delta\sigma_h$) from the experimental and computational results with respect to the V for each type of U-loop expansion pipe. The results indicate that the characteristic patterns for each U-loop type are similar, with $\Delta\sigma_h$ increasing from 5.0 m/s to 7.0 m/s. The hoop stress reduction values at each water flow velocity level were the highest for Type 1, followed by Type 3, and the lowest for Type 2. This characteristic pattern aligns with the experimental pressure reduction patterns at each velocity level.

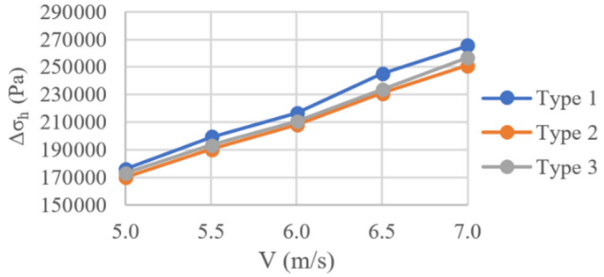

Fig. 13. Distribution of $\Delta\sigma_h$ with V for all types of U-Loop expansion pipes.

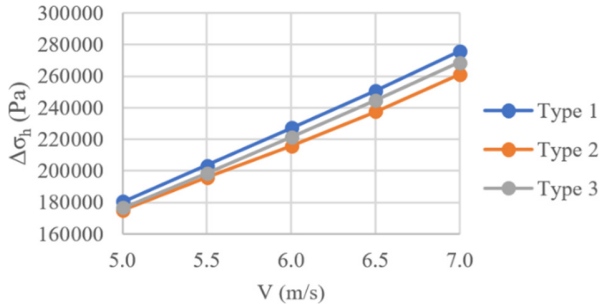

Fig. 14. Computational results of $\Delta\sigma_h$ with V for all types of U-Loop expansion pipes.

Figure 15 illustrates the hoop stress reduction (Δσh) versus the flow velocity (V) for each U-loop expansion pipe. The experimental and computational results displayed similar trends, with an average difference of approximately 4%, while the computational values were consistently higher than the experimental ones.

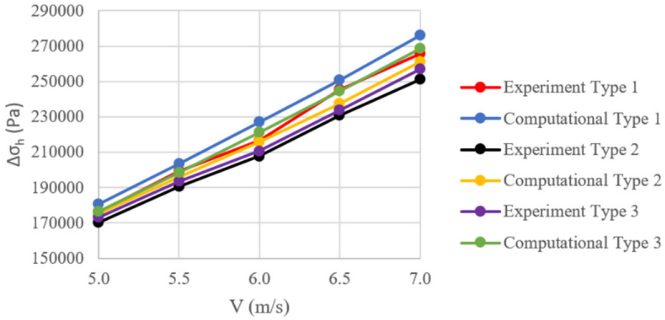

Fig. 15. Experimental and computational hoop stress reduction ($\Delta\sigma_h$) with V for all types of U-Loop expansion pipes.

Figures 16 and 17 display the longitudinal stress reduction (Δσl) versus the flow velocity (V) for each U-loop expansion pipe. Both the experimental and computational results exhibited the same trend, with Δσl increasing from 5.0 to 7.0 m/s. Type 1 showed the highest values, followed by Type 3, and Type 2 demonstrated the lowest values, which is consistent with the pressure reduction patterns.

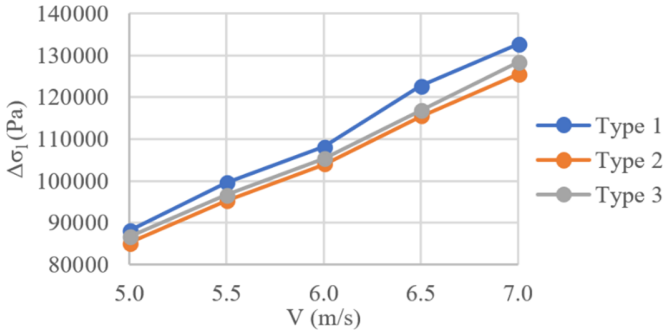

Fig. 16. Results of experiments on longitudinal stress reduction ($\Delta\sigma_l$) against V for each type of U-Loop expansion pipe.

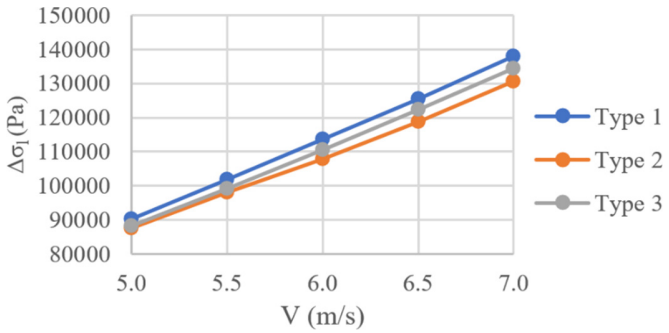

Fig. 17. Computational results of $\Delta\sigma_l$ against V for each type of U-Loop expansion pipe.

Figure 18 shows the longitudinal stress reduction (Δσl) versus the flow velocity (V) for each U-loop expansion pipe type, with the experimental and computational results exhibiting similar trends. The average difference was approximately 4%, with the computational values being consistently higher than the experimental values.

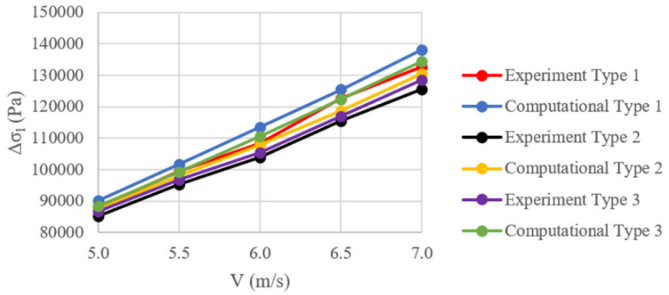

Fig. 18. Longitudinal stress reduction ($\Delta\sigma_l$) from experiments and computations with V for each type of U-Loop expansion pipe.

Figures 19 and 20 show the hoop and longitudinal stress distributions obtained from the experimental and computational results, respectively, for the U-loop expansion pipe at a flow velocity of 7 m/s. Both methods showed similar trends, with the average stress values differing by approximately 3%. In all cases, the computational results were slightly higher than the experimental results at the same measurement points.

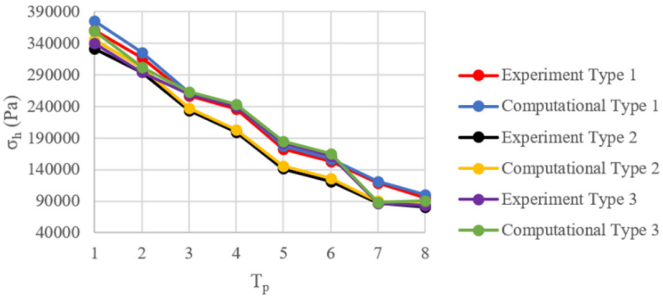

Fig. 19. Distribution of hoop stress (σ_h) from experiments and computations relative to T_P for each type of U-Loop expansion pipe at a velocity V = 7 m/s.

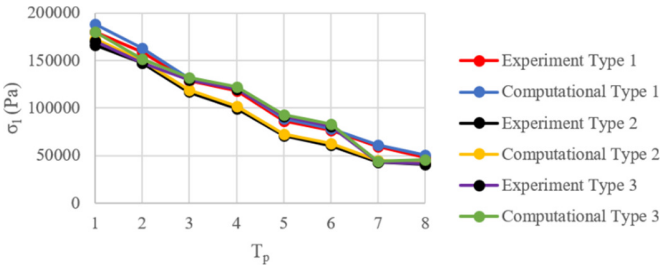

Fig. 20. Distribution of σ_l from experiments and computations relative to T_P for each type of U-Loop expansion pipe at a velocity V = 7 m/s.

Figures 21-23 present the static pressure contours for Types 1-3 U-loop expansion pipes, respectively, at a water flow velocity of 7 m/s. The pressure drop at each elbow exhibited the same pattern for each type; however, the largest pressure drop occurred on the outlet side or elbow 4 of Type 1 pipe. These contour results are consistent with both the experimental pressure drop and the computational results.

IV. CONCLUSIONS

This study presents the computational and experimental results on the characteristics of water flow in U-loop expansion pipes, focusing on pressure distribution, circumferential stress, and longitudinal stress. Three types of U-loop models were tested with flow velocity variations from 5.0 m/s to 7.0 m/s. The results show that an increase in flow velocity results in a greater decrease in pressure, circumferential stress, and longitudinal stress in all types of U-loops, with Type 1 showing the greatest reduction compared to Types 3 and 2. The validation between the computational and experimental results showed a consistent pattern with an average difference of approximately 3%, where the computational values were slightly higher than the experimental results.

The knowledge gap addressed by this research is the limited number of studies that simultaneously analyze the pressure distribution and structural stress response in U-loop expansion pipes. The main scientific contribution of the present work is to provide a new understanding of the direct relationship between the flow characteristics and structural stress changes, which was validated through a combined computational-experimental approach. The novelty of this study lies in the integrated analysis of pressure and stress in a single system, which has not been widely studied because most previous studies have focused on only one aspect.

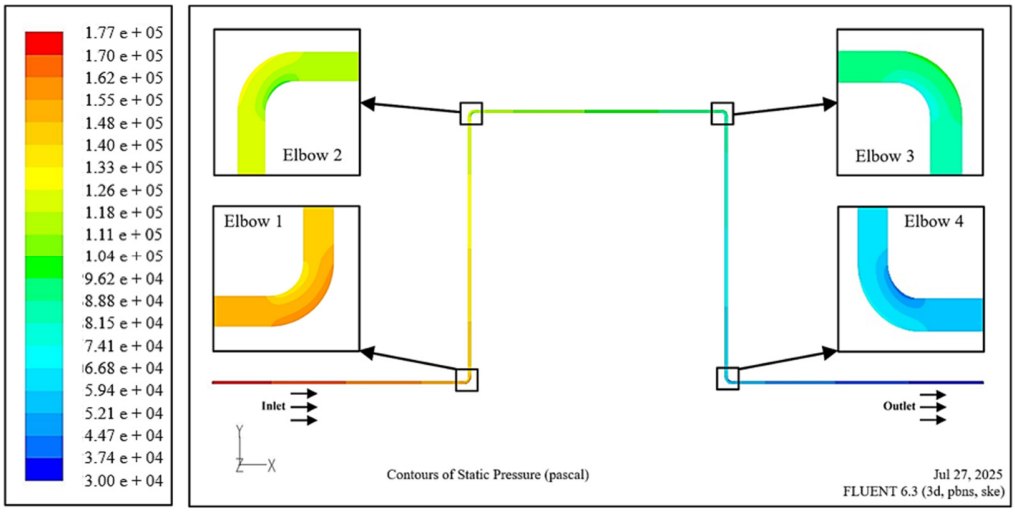

Fig. 21. Static pressure contour of Type 1 U-Loop expansion pipe at a water flow velocity of V = 7 m/s.

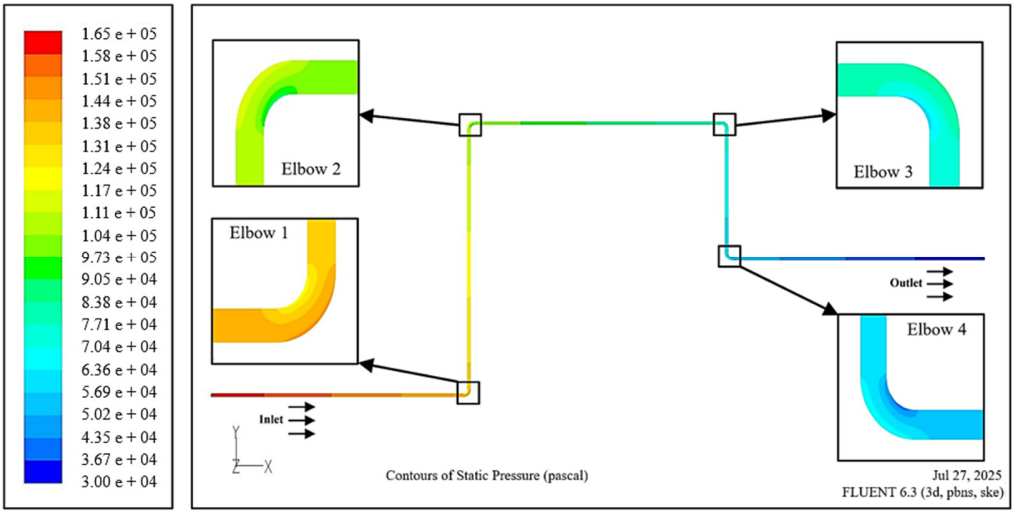

Fig. 22. Static pressure contour of Type 2 U-Loop expansion pipe at a water flow velocity of V = 7 m/s.

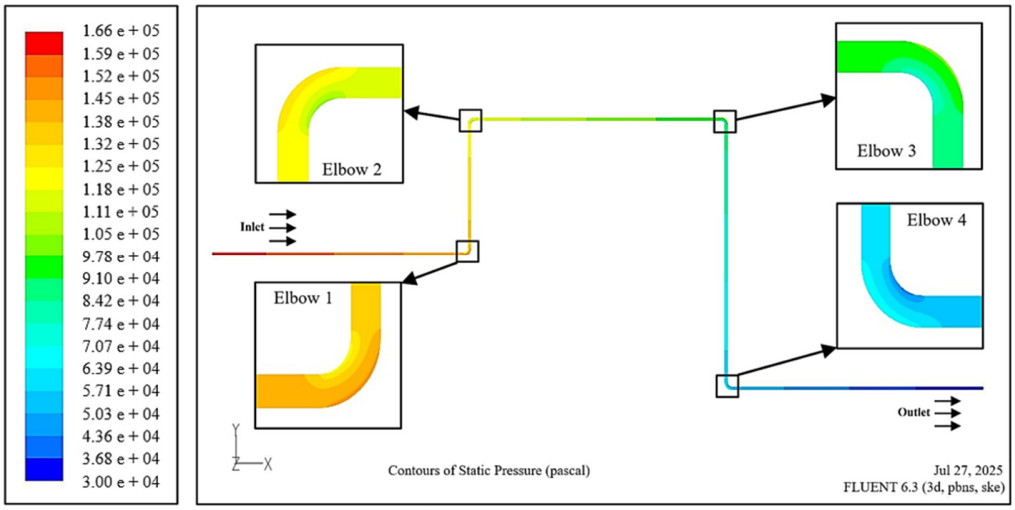

Fig. 23. Static pressure contour of Type 3 U-Loop expansion pipe at a water flow velocity of V = 7 m/s.

A strong consistency between the computational and experimental results is demonstrated, confirming the reliability of the combined approach. In addition, the superior performance of the Type 1 configuration in reducing the pressure, hoop stress, and longitudinal stress provides a solid reference for optimizing the design of U-loop pipes to improve the flow efficiency.

ACKNOWLEDGMENTS

The authors would like to express their gratitude to the Rector of Hasanuddin University and the Research and Community Service Institute (LP2M) of Hasanuddin University for funding this research through the Thematic Research Group (TRG) Batch 2 Grant of Hasanuddin University for the 2025 Fiscal Year, contract number 00773/UN4. 22/PT.01.03/2025 and to the administrators of the Fluid Mechanics Laboratory, Department of Mechanical Engineering, Faculty of Engineering, Hasanuddin University, for granting permission and facilitating this research.

REFERENCES

[1] M. A. W. Adhicahya, N. Salam, and R. Tarakka, "Pipe Stress Analysis of Pertalite Fuel Discharge Pipeline PT Pertamina Patra Niaga Integrated Terminal Makassar," *Prosiding Seminar Nasional Tahunan Teknik Mesin*, vol. 21, pp. 160–167.

[2] P. Mahardhika, A. W. Husodo, G. E. Kusuma, R. D. E. Witjonarko, and E. N. Budiyanto, "Analysis of Symmetrical and Nonsymmetrical Vertical Expansion Loop to Increase Flexibility And Reduce Pipe Stress Based On ASME B31.3," *TEKNIK*, vol. 42, no. 1, pp. 63–70, May 2021, https://doi.org/10.14710/teknik.v42i1.29244.

[3] M. Haq and B. Riyandwita, "Analysis of the Effect of Variations in Expansion Loop Shapes on Pressure Drops Occurring in the Flow of Crude Oil in Pipeline Using Computational Fluid Dynamics," presented at International Conference on Sustainable Engineering, Infrastructure and Development, ICO-SEID 2022, Jakarta, Indonesia, Dec. 2023, https://doi.org/10.4108/eai.23-11-2022.2341543.

[4] Y. Elahibakhsh, "Innovative Approaches to Expansion Loop Design for Enhanced Piping System Durability," *American Journal of Mechanical and Materials Engineering*, vol. 8, no. 2, pp. 25–32, Sep. 2024, https://doi.org/10.11648/j.ajmme.20240802.11.

[5] P. Pujiyanto, H. Yudo, and S. J. Sisworo, "Desain dan Analisa Kekuatan Pipa Expansion Loops dengan Variasi Ukuran Loop dan Bentuk Loop," *Jurnal Teknik Perkapalan*, vol. 9, no. 2, pp. 145–151, Jan. 2021.

[6] T. F. Nugroho, E. M. Wardhana, and R. N. Azmi, "Stress Analysis of Land Subsidence Effect on Header Pipe 12 Inch in LPG Station Semarang," *International Journal of Marine Engineering Innovation and Research*, vol. 2, no. 4, pp. 261–268, Sep. 2018, https://doi.org/10.12962/j25481479.v2i4.4069.

[7] *ASME B31.3 Process Piping Guide*. American Society of Mechanical Engineers, 2012.

[8] H. Yudo, S. Jokosisworo, W. Amiruddin, P. Pujianto, T. Tuswan, and M. Djaeni, "Numerical evaluation of expansion loops for pipe subjected to thermal displacements," *Curved and Layered Structures*, vol. 9, no. 1, pp. 72–80, Jan. 2022, https://doi.org/10.1515/cls-2022-0007.

[9] B. Shehadeh, S. I. Ranganathan, and F. H. Abed, "Optimization of piping expansion loops using ASME B31.3," *Proceedings of the Institution of Mechanical Engineers, Part E: Journal of Process Mechanical Engineering*, vol. 230, no. 1, pp. 56–64, Feb. 2016, https://doi.org/10.1177/0954408914532808.

[10] C. Cholca, W. Quitiaquez, E. Pilataxi, and F. Toapanta, "Evaluation of Flexible Configuration Pipeline Networks for Hydrocarbon Transportation," *Revista Técnica energía*, vol. 20, no. 1, pp. 100–108, Dec. 2023, https://doi.org/10.37116/revistaenergia.v20.n1.2023.583.

[11] B. Debtera, "Computational Fluid Dynamics Simulation and Analysis of Fluid Flow in Pipe: Effect of Fluid Viscosity," *Social Science Research Network*, Aug. 2022, https://doi.org/10.2139/ssrn.4201717.

[12] R. K. Apalowo and C. J. Akisin, "CFD-based investigation of turbulent flow behavior in 90-deg pipe bends," *Journal of Applied Research in Technology & Engineering*, vol. 5, no. 2, pp. 53–62, Mar. 2024, https://doi.org/10.4995/jarte.2024.20665.

[13] M. W. Khalid and M. Ahsan, "Computational Fluid Dynamics Analysis of Compressible Flow Through a Converging-Diverging Nozzle using the k-ε Turbulence Model," *Engineering, Technology & Applied Science Research*, vol. 10, no. 1, pp. 5180–5185, Feb. 2020, https://doi.org/10.48084/etasr.3140.

[14] O. Y. Wei and S. U. Masuri, "Computational Fluid Dynamics Analysis on Single Leak and Double Leaks Subsea Pipeline Leakage," *CFD Letters*, vol. 11, no. 2, pp. 95–107, 2019.

[15] M. A. Asri *et al.*, "Flow Characteristics for Leak Detection in Oil and Gas Pipeline Network Using CFD Simulations," *Journal of Design for Sustainable and Environment*, vol. 4, no. 1, pp. 1–8, 2022.

[16] A. A. Abuhatira, S. M. Salim, and J. B. Vorstius, "CFD-FEA based model to predict leak-points in a 90-degree pipe elbow," *Engineering with Computers*, vol. 39, no. 6, pp. 3941–3954, Dec. 2023, https://doi.org/10.1007/s00366-023-01853-4.

[17] H. Fu, L. Yang, H. Liang, S. Wang, and K. Ling, "Diagnosis of the single leakage in the fluid pipeline through experimental study and CFD simulation," *Journal of Petroleum Science and Engineering*, vol. 193, Oct. 2020, Art. no. 107437, https://doi.org/10.1016/j.petrol.2020.107437.

[18] L. C. Peng and T. L. Peng, *Pipe Stress Engineering*. American Society of Mechanical Engineers, 2009.

[19] P. F. Mushumbusi, A. Chaudhari, J. Leo, and V. G. Masanja, "CFD Analysis of Flow Characteristics and Diagnostics of Leaks in Water Pipelines," *Engineering, Technology & Applied Science Research*, vol. 14, no. 5, pp. 16272–16280, Oct. 2024, https://doi.org/10.48084/etasr.8146.

[20] Z. Huda and M. H. Ajani, "Evaluation of Longitudinal and Hoop Stresses and a Critical Study of Factor of Safety (FoS) in Design of a Glass-Fiber Pressure Vessel," *International Journal of Materials and Metallurgical Engineering*, vol. 9, no. 1, pp. 39–42, Jan. 2015.